

## Analyzing data from DASI

Martin White<sup>1</sup>, John Carlstrom<sup>2</sup>, Mark Dragovan<sup>3</sup>, S.W.L. Holzapel<sup>4</sup>

<sup>1</sup>Harvard-Smithsonian Center for Astrophysics  
60 Garden St, Cambridge, MA 02138

<sup>2</sup>Department of Astronomy and Astrophysics, University of Chicago  
5621 South Ellis Ave, Chicago IL 60637

<sup>3</sup>Jet Propulsion Laboratory, Pasadena, CA91109

<sup>4</sup>University of California, Berkeley, CA 94720

### ABSTRACT

We present an optimized layout of horn positions for the Degree Angular Scale Interferometer (DASI), which provides good coverage of the  $u$ - $v$  plane and 3-fold symmetry. We investigate how an optimal subspace filtering analysis of a single pointing of DASI could be used to determine the anisotropies in the cosmic microwave background over a range of angular scales near  $30'$ . We discuss the complementarity between the angular scales probed by DASI and NASA's MAP satellite at 30GHz and strategies for imaging the sky at these frequencies. Finally, we quantitatively assess how well the angular power spectrum can be recovered by deconvolution of linear combinations of squares of the DASI visibilities.

*Subject headings:* cosmology:theory – cosmic microwave background

### 1. Introduction

The study of the Cosmic Microwave Background (CMB) anisotropy holds the promise of answering many of our fundamental questions about the universe and the origin of the large-scale structure (see e.g. Bennett, Turner & White 1997). The advent of low-noise, broadband, millimeter-wave amplifiers (Popieszalski 1993) has made interferometry a particularly attractive technique for detecting and imaging low contrast emission, such as anisotropy in the CMB. An interferometer directly measures the Fourier transform of the intensity distribution on the sky. By inverting the interferometer output, images of the sky are obtained which include angular scales determined by the size and spacing of the individual array elements.

In an earlier paper (White et al. 1998, hereafter WCDH) we outlined a formalism for interpreting CMB anisotropies as measured by interferometers. In this paper we extend this analysis to consider an efficient method of analyzing the data that would be obtained from a series of uncorrelated pointings of an interferometer. In particular we examine what the upcoming Degree Angular Scale Interferometer<sup>1</sup> (DASI, Halverson et al. 1998) experiment may teach us about cosmology.

DASI is an interferometer designed to measure anisotropies in the CMB over a large range of scales with high sensitivity. The array consists of 13 closely packed elements, each of 20cm diameter, in a configuration which fills roughly half of the aperture area with a 3-fold symmetry. Each element of the array is a wide-angle corrugated horn with a collimating lens. DASI uses cooled HEMT amplifiers running between 26-36GHz

---

<sup>1</sup>More information on DASI can be found at <http://astro.uchicago.edu/dasi>.

with a noise temperature of  $< 15\text{K}$ . The signal is filtered into ten 1GHz channels. Details of the layout of the DASI horns is given below.

The outline of this paper is as follows. In §2 we adapt the formalism of WCDH to deal with real and imaginary parts of the visibilities independently, and show explicitly how the formalism automatically imposes the constraint that the sky temperature is real. With the issues defined, we describe the configuration of DASI in §3. In §4, 5 we analyze mock data appropriate to single fields from DASI, showing how to construct an optimal basis for likelihood analysis. We specifically address the question of optimal sampling on the sky, which was omitted from our previous work. This leads naturally to a discussion of Wiener filtered (Bunn, Hoffman & Silk 1996) map making and we reformulate the strategy for imaging the sky in this basis, pointing out the complementarity between NASAs *MAP* satellite<sup>2</sup> and DASI at 30GHz. We discuss estimates of the angular power spectrum which are easy to implement for uncorrelated pointing of DASI in §6 and show that the finite field of view does not hamper our ability to reconstruct the angular power spectrum. Finally in §7 we discuss multi-frequency observations and present our power spectrum results in the context of “radical compression” (Bond, Jaffe & Knox 1998).

## 2. Formalism

The reader is referred to our earlier paper (WCDH) for a detailed discussion of how to formulate the data-analysis problem with an interferometer, plus references to earlier work. We briefly review the major elements here.

Under the assumption of a narrow frequency band and a distant source, the datum measured by an interferometer is proportional to the Fourier Transform of the observed intensity on the sky, i.e. the sky intensity multiplied by the instrument beam. We label the “primary” beam of the telescope by  $A(\mathbf{x})$ , with  $\mathbf{x}$  a 2D vector lying in the plane<sup>3</sup> of the sky. Every pair of telescopes in the interferometer measures a visibility at a given point in the Fourier Plane, called the  $u - v$  plane,

$$\mathcal{V}(\mathbf{u}) \propto \int d\mathbf{x} A(\mathbf{x})\Delta T(\mathbf{x})e^{2\pi i\mathbf{u}\cdot\mathbf{x}} \quad (1)$$

where  $\Delta T$  is the temperature (fluctuation) on the sky and  $\mathbf{u}$  is the variable conjugate to  $\mathbf{x}$ , with dimensions of inverse angle measured in wavelengths. The (omitted) proportionality constant,  $\partial B_\nu/\partial T$  where  $B_\nu$  is the Planck function, converts from temperature to intensity. The spacing of the horns and the position of the beam on the sky determine which value of  $\mathbf{u}$  will be measured by a pair of antennae in any one integration. The size of the primary beam determines the amount of sky that is viewed, and hence the size of the “map”, while the maximum spacing determines the resolution.

The 2-point function of the observed visibilities is the convolution of the sky power spectrum,  $S(\mathbf{u}, \mathbf{v})$ , with the Fourier Transforms of the primary beams. If our theory is rotationally invariant the power spectrum is diagonal,  $S(\mathbf{u}, \mathbf{v}) = S(u)\delta(\mathbf{u} - \mathbf{v})$  and on small scales (WCDH)

$$u^2 S(u) \simeq \frac{\ell(\ell+1)}{(2\pi)^2} C_\ell \Big|_{\ell=2\pi u} \quad \text{for } u \gtrsim 10 \quad . \quad (2)$$

---

<sup>2</sup><http://map.gsfc.nasa.gov/>

<sup>3</sup>Since the field of view of the currently operational or planned instruments is small ( $\lesssim 5^\circ$ ) the sky can be approximated as flat with excellent accuracy.

where the dimensionless  $C_\ell$  are the usual multipole moments of the CMB anisotropy spectrum and  $\ell \sim \theta^{-1}$  is the multipole index. This approximation works at the few percent level for a standard Cold Dark Matter model when  $u \gtrsim 10$  or  $\ell \gtrsim 60$ .

The Fourier Transform of the primary beam<sup>4</sup> is the auto-correlation of the Fourier Transform of the point response,  $g$ , of the receiver to an electric field,  $\tilde{A}(u) = \tilde{g} \star \tilde{g}(u)$  and

$$A(\mathbf{x}) = \int d\mathbf{u} \tilde{A}(\mathbf{u}) e^{-2\pi i \mathbf{u} \cdot \mathbf{x}} \quad , \quad (3)$$

Due to the finite aperture  $\tilde{A}$  has compact support. In order to obtain a simple estimate of our window function it is a reasonable first approximation to take  $\tilde{A}$  equal to the auto-correlation of a pill-box of radius  $D/2$  where  $D$  is the diameter of the dish in units of the observing wavelength. Specifically

$$\tilde{A}(\mathbf{u}) = \frac{2\tilde{A}_*}{\pi} \left[ \arccos \frac{u}{D} - \frac{u\sqrt{D^2 - u^2}}{D^2} \right] \quad (4)$$

if  $u \leq D$  and zero otherwise. If we require  $A(0) = 1$  then this must integrate to unit area, so  $\tilde{A}_*^{-1} = \pi(D/2)^2$ , or the area of the dish. We show  $\tilde{A}(u)$  in Fig. 2a. For now we shall treat a single frequency. Obviously for a fixed physical dish the  $\tilde{A}$  will be slightly different for different wavelengths. We return to this complication in §7.

In WCDH we presented the formalism in terms of complex visibility data. However it is easier practically to implement the analysis in terms of the real and imaginary parts of the visibility. We write these as  $\mathcal{V}_j \equiv V_j^R + iV_j^I$ . The cosmological contribution to the real and imaginary components is uncorrelated  $\langle V_i^R V_j^I \rangle = 0$ . Assemble  $V^R$  and  $V^I$  into a vector consisting of first the real and then the imaginary parts – the signal correlation matrix of this vector takes block-diagonal form. Further the cosmological contribution obeys  $\langle V_i^R V_j^R \rangle = \pm \langle V_i^I V_j^I \rangle$ . It is straightforward to show that the cosmological contribution is proportional to

$$\frac{1}{2} \int d\mathbf{v} S(v) \tilde{A}(\mathbf{u}_i - \mathbf{v}) \left[ \tilde{A}(\mathbf{u}_j - \mathbf{v}) \pm \tilde{A}(\mathbf{u}_j + \mathbf{v}) \right] \quad (5)$$

where the  $\pm$  refer to the real and imaginary parts respectively. (We have dropped the normalization factor which converts temperature to flux.) Note that if  $\mathbf{u}_i = -\mathbf{u}_j$  the visibilities are completely (anti-)correlated, as would be expected given that  $\mathcal{V}(\mathbf{u})$  is the Fourier Transform of a real field:  $\mathcal{V}^*(\mathbf{u}) = \mathcal{V}(-\mathbf{u})$ . The factor of  $\frac{1}{2}$  out front reflects the fact that the full variance  $C_{ij}^V \equiv \langle \mathcal{V}_i^* \mathcal{V}_j \rangle$  is the sum of the real and imaginary components.

In the case where all correlated signal is celestial, the correlation function of the noise in each visibility is diagonal with

$$C_{ij}^N = \left( \frac{2k_B T_{\text{sys}}}{\eta_A A_D} \right)^2 \frac{1}{\Delta_\nu t_a n_b} \delta_{ij} \quad . \quad (6)$$

If the noise in the real and imaginary components is uncorrelated, then each makes up half of this variance. Here  $k_B$  is Boltzmann's constant,  $T_{\text{sys}}$  is the system noise temperature,  $\eta_A$  is the aperture efficiency,  $A_D$  is the physical area of a dish (not to be confused with  $A(\mathbf{x})$ ),  $n_b$  is the number of baselines<sup>5</sup> corresponding to

<sup>4</sup>Throughout we will use a tilde to represent the Fourier Transform of a quantity.

<sup>5</sup>The number of baselines formed by  $n_r$  receivers is  $n_b = n_r(n_r - 1)/2$ .

a given separation of antennae,  $\Delta_\nu$  is the bandwidth and  $t_a$  is the observing time. Typical values for DASI are  $T_{\text{sys}} = 20\text{K}$ ,  $\eta_A \sim 0.8$ , dishes of diameter 20cm,  $n_b = 3$  and  $\Delta_\nu = 10\text{GHz}$  (in  $10 \times 1\text{GHz}$  channels).

We show in Fig. 1 the positions at which DASI will measure visibilities. With 13 horns there are 78 baselines. Because of the 3-fold symmetry of the instrument each pointing samples  $V$  at 26 different  $|\mathbf{u}|$ . For each “stare” DASI is rotated about an axis perpendicular to the baseplate to fill half of the  $u - v$  plane as shown in Fig. 1. The other half of the  $u - v$  plane is constrained by the symmetry  $\mathcal{V}^*(\mathbf{u}) = \mathcal{V}(-\mathbf{u})$ .

### 3. The DASI configuration

The layout of the horns for DASI is shown in Fig. 1a. This configuration has a 3-fold symmetry about the central horn. The positions of 4 of the non-central horns are arbitrary, up to a global rotation, with the remaining configuration being determined by symmetry. The configuration shown represents an optimal configuration, within the physical constraints, for the purposes of measuring CMB anisotropy.

As described in the last section, the distance between each pair of horns represents a baseline at which a visibility can be measured. Each visibility probes a range of angular scales centered at  $\ell = 2\pi u$  where  $u$  is the baseline in units of the wavelength. The sensitivity as a function of  $\ell$  is given by the window function (see Eq. 8). Since the width of the window function is determined by the size of the apertures, the optimal coverage for the purpose of CMB anisotropy is that configuration which spans the largest range of baselines with the most overlap between neighbouring window functions. In one dimension such optimal configurations are known as Golomb<sup>6</sup> rulers (Dewdney 1985), and a well known procedure exists for finding them.

Finding an optimal solution in two dimensions, within the physical constraints, cannot be done analytically. We have optimized the configuration numerically. We have searched the 7 dimensional parameter space of horn positions (an  $x$  and  $y$  position for each of 4 horns, minus one overall rotation) for the configuration which minimized the maximum separation between baseline distances, while at the same time covering the largest range of angular scales. Trial starting positions were determined by a simple Monte Carlo search of the parameter space. From each of these positions a multi-dimensional minimization was started. Two additional constraints were imposed upon the allowed solutions: no two horns could come closer than 25cm, the physical size of the horn plus surrounding “lip”, and all horns etc had to lie completely within the 1.6m diameter base plate (leading to a maximal radius of 63.5cm). Our “optimal” solution is given in Table 1. The baselines run from 25cm to 120cm with the largest gap between baseline distances being 6.4cm.

### 4. S/N Eigenmodes or Optimal Subspace Filtering

A quick glance at Fig. 1b shows that the signal in most of the visibilities will be highly correlated, i.e. the apertures have a large overlap. This is shown quantitatively in Fig. 3a where we plot one row of the signal correlation matrix. Given a “trial” theory we can perform a change of basis to remove these correlations (see §6.2 of WCDH, or Tegmark et al. 1998 for a review of this method). The input theory can be considered as a prior in the context of Bayesian analysis, or could be iterated to match the data if so desired. For our purposes all that will matter is that the signal variance is independent of  $\hat{u}$  and decreases with  $|\mathbf{u}|$ . For

---

<sup>6</sup>e.g. <http://members.aol.com/golomb20/>

concreteness we will take  $u^2 S(u) = \text{constant}$ , normalized to the COBE 4-year data (Bennett et al. 1996). For this choice the cosmological signal is approximately equal to the noise in each of the highest  $|\mathbf{u}|$  bins in Fig. 1b.

Let us consider only the real parts of the visibilities for now, the imaginary parts are dealt with in an analogous manner. Take these to lie in the upper-left block of the block-diagonal correlation matrix. Denote the noise in the real part of each visibility  $\sigma_j$ . The eigenvalues of the matrix  $C_{ij}^{RR}/\sigma_i\sigma_j$  measure the signal-to-noise in *independent* linear combinations of the visibilities. The independent linear combinations can be written  $\nu_a = \sum_i (V_i/\sigma_i)\Psi_{ia}$  where  $\Psi_{ia}$  is the  $a$ th eigenvector of  $C_{ij}^{RR}/\sigma_i\sigma_j$ . Then  $\langle \nu_a \nu_b \rangle = (\lambda_a + 1)\delta_{ab}$  where the  $\lambda_a$  are the signal-to-noise eigenvalues and the 1 represents the noise contribution (which is the unit matrix in this basis).

The number of modes  $\nu_a$  with  $\lambda_a > 1$  is a quantitative indication of how much signal is being measured by the experiment. We show the eigenspectrum of the *real* parts of the visibilities for 1 day of observation in Fig. 3b. There is in addition an eigenvalue of the same size for each imaginary component. Due to the overlapping windows in the  $u - v$  plane,  $\lesssim 25\%$  of the modes contain good cosmological information. The rest are redundant, containing mostly noise. Note however that in 1 day of observation DASI measures nearly 200 high signal-to-noise eigenvectors! We have tested that reducing the number of orientations of the instrument, i.e. the oversampling in  $\theta_u$ , does not significantly reduce the number of high signal-to-noise eigenvectors until the apertures in the outermost circle are just touching, at which point there are 160 modes with  $S/N \gtrsim 1$ .

The  $\lambda_a$  are the variance of the  $\nu_a$  and can be predicted given a theoretical power spectrum

$$\lambda_a = \frac{1}{2} \int v dv S(v) W_a(v) \quad (7)$$

with the window function

$$W_a(|\mathbf{v}|) = \sum_{ij} \frac{\Psi_{ia}}{\sigma_i} \frac{\Psi_{ja}}{\sigma_j} \int d\theta_v \tilde{A}(\mathbf{u}_i - \mathbf{v}) \left[ \tilde{A}(\mathbf{u}_j - \mathbf{v}) \pm \tilde{A}(\mathbf{u}_j + \mathbf{v}) \right] \quad (8)$$

and as such could form a basis for “radical compression”. We shall return to this issue in §7.

## 5. Imaging the Sky

DASI provides coverage over a significant part of the  $u - v$  plane, and as such is able in principle to perform high resolution imaging of the sky. The high signal to noise of the DASI instrument and the large dynamic range in angular scale however make imaging a computationally challenging task. In this section we present two approaches which we have tried with mixed success on simulated data.

We discussed the Wiener filtering formalism for producing an image from the visibility data in WCDH. Here we note that in the  $\nu_a$  basis it is straightforward to construct the Wiener filtered sky map (Bunn, Hoffman & Silk 1996; WCDH and references therein). Recall that for Wiener filtering the sky temperature is approximated by

$$T^{WF}(\mathbf{x}_\alpha) = C_{\alpha\beta}^T W_{\beta j} [C^V + C^N]_{jk}^{-1} V_k \quad (9)$$

where  $C^T$  is the real-space temperature correlation function,

$$W_{\beta j} = A(\mathbf{x}_\beta) \left\{ \begin{array}{c} \cos \\ \sin \end{array} \right\} [2\pi i \mathbf{u}_j \cdot \mathbf{x}_\beta] \quad (10)$$

we choose cos for the real components and sin for the imaginary components, and  $C^V$  and  $C^N$  are the visibility signal and noise correlation matrices. We have written the expression in this mixed way to avoid needing to invert a matrix of size  $N_{\text{pix}} \times N_{\text{vis}}$  where  $N_{\text{pix}}$  is the number of pixels in the map being reconstructed, but conceptually the  $C^T W$  term can be replaced with  $W^{-1} C^V$ . Then in the  $\nu_a$  basis one simply replaces  $\nu_a$  with  $\lambda_a(\lambda_a + 1)^{-1} \nu_a$  which down-weights modes with low signal-to-noise. Specifically

$$T^{WF}(\mathbf{x}_\beta) = \sum_a M_{\beta a}^{-1} \frac{\lambda_a}{\lambda_a + 1} \nu_a \quad (11)$$

where

$$M_{\beta a} = \sum_j \frac{\Psi_{ja}}{\sigma_j} A(\mathbf{x}_\beta) \begin{Bmatrix} \text{cos} \\ \text{sin} \end{Bmatrix} [2\pi i \mathbf{u}_j \cdot \mathbf{x}_\beta] \quad (12)$$

where we choose cos for the real components and sin for the imaginary components. The ratio  $\lambda_a(\lambda_a + 1)^{-1}$  is plotted in Fig. 3b, where we can see that  $\lesssim 25\%$  of the modes will contribute significantly to the final map. The expected variance in the final map is also easily computed:

$$\langle T_\rho^{WF} T_\sigma^{WF} \rangle = \sum_a M_{\rho a}^{-1} \frac{\lambda_a^2}{\lambda_a + 1} M_{a\sigma}^{-1} \quad (13)$$

which approaches  $\langle T^2 \rangle$  as  $\lambda_a \rightarrow \infty$ . Note that the Wiener filter is *not* power preserving, so the maps should not be used for power spectrum estimation.

By reducing the total number of modes that need to be kept in the summation the  $\nu_a$  basis can speed up calculation of the Wiener filtered map. This is an advantage, but even with this speed up we found that producing a high resolution map of even a single field on the sky is very computationally expensive due to the large number of matrix multiplications involved in computing  $T^{WF}$ . An alternative to Wiener filtering, which is very similar in the high signal-to-noise regime in which we are working, is the minimum variance estimator for  $T(\mathbf{x})$ . The number of operations required to produce the minimum variance and Wiener filtered maps are comparable, and both tend to be very slow. We are currently investigating faster approximate methods of image making.

The formalism above can in principle be used for making maps at each frequency, or one can make a map which combines the frequencies in such a way as to isolate the CMB (or foreground) signal. While the formalism looks more complex, it is in fact easy to implement computationally. The techniques are well known (see §7): we imagine that at each point in the  $u - v$  plane our visibilities form a vector  $\vec{V}$  whose components are the different frequencies. We can expand this vector in terms of the physical components we wish to consider, e.g.,

$$\vec{V} = \theta_{\text{CMB}} \vec{V}^{\text{CMB}} + \theta_{ff} \vec{V}^{ff} \quad (14)$$

In the absence of noise it is easy to solve for  $\theta_{\text{CMB}}$  as

$$\theta_{\text{CMB}} = \frac{\vec{V}_\perp \cdot \vec{V}}{\vec{V}_\perp \cdot \vec{V}^{\text{CMB}}} \quad \text{with} \quad \vec{V}_\perp \cdot \vec{V}^{ff} = 0 \quad (15)$$

If we write  $\theta_{\text{CMB}} = \sum_a c_a V_a$  then we should replace  $\tilde{A}$  by  $\sum_a c_a \tilde{A}_a$  throughout. In the presence of noise we may define  $c_a$  by a minimum variance estimator as above:

$$c_a = \sum_A \left( \sum_{bc} V_b^{\text{CMB}} N_{bc}^{-1} V_c^A \right)^{-1} \sum_d V_d^A N_{da}^{-1} \quad (16)$$

where  $N_{ab}$  is the channel noise matrix and capital Roman letters indicate the component being considered (see §7).

We end our discussion of imaging with an observation about the complementarity between the *MAP* satellite and DASI. In making maps of the sky with DASI, the largest source of error is the missing long wavelength modes which are filtered out by the DASI primary beam. The long wavelength power can be included in the map by simultaneously fitting another data set (e.g. WCDH). In this particular case the data from the *MAP* satellite at the same frequency is the obvious choice since *MAP* will have full sky coverage. We show the window functions for *MAP* at the relevant frequencies, along with the envelope for DASI in Fig. 4.

## 6. Power Spectrum Estimation

While the  $\nu_a$  are the natural basis from the point of view of signal-to-noise and Wiener filtering, and can dramatically improve likelihood function evaluation, they are not necessarily the quantities of greatest physical interest for power spectrum estimation. In WCDH we discussed estimating a series of bandpowers using the quadratic estimator of (Bond, Jaffe & Knox 1998, Tegmark 1997). Here we present a simpler approach more appropriate to unmosaiced fields. In this presentation we shall assume we are dealing with single frequencies; the case of multiple frequencies is dealt with in §7.

In CMB anisotropy observations with single dish experiments much has been written about optimal ways to estimate the power spectrum. The principle reason is that care must be taken in weighting the data to ensure that no sharp cut-offs in real space are introduced. These lead to ringing in Fourier space and delocalize the window function (e.g. discussion in Tegmark 1996). For the interferometer no such problem arises – each visibility samples a compact region in  $\mathbf{u}$ . For each  $V_i$ , the square is a noise biased estimate of the power spectrum convolved with a window function. If we define  $s_i \equiv 2(V_i^2 - N_{ii})$  with  $N_{ii}$  the noise variance in (the component of the) visibility  $i$ , then  $s_i$  is an unbiased estimator for  $C_{ii}^V$ :

$$\langle s_i \rangle = \int u du S(u) W_{ii}(u) \quad (17)$$

where  $W_{ii}(u)$  is the window function in analogy to Eq. (8). We have included the factor of 2 in the definition of  $s_i$  to account for the fact that each component  $V_i$  of the visibility contributes half of the total variance of  $|\mathcal{V}_i|^2$ . Take a weighted average of the  $s_i$ :  $\mathcal{S}_A \equiv E_{Ai} s_i$ . The simplest weighting is to sum all of the  $s_i$  with  $|\mathbf{u}_i| \simeq u$  and we shall use that below. Under the assumption that the visibilities are Gaussian, the error matrix for the estimates  $\mathcal{S}_A$  is

$$\langle \delta \mathcal{S}_A \delta \mathcal{S}_B \rangle = 2 \sum_{ij} E_{Ai} (C_{ij}^V + C_{ij}^N)^2 E_{jB} \quad . \quad (18)$$

Note that for  $N$  uncorrelated visibilities (real and imaginary parts) contributing to  $\mathcal{S}_A$  this gives  $\delta \mathcal{S}_A / \mathcal{S}_A = N^{-1/2}(1 + \text{noise/signal})$  as expected.

For DASI in the configuration shown in Fig. 1b one can construct 26 different estimates  $\mathcal{S}_A$ , which will however be quite correlated. We show the  $13 \times 13$  correlation matrix for every *second* estimate in Table 2 along with the expected error on each determination (the diagonal elements). As independent pointings are included in the analysis the error bar on each  $\mathcal{S}_A$  decreases as  $N^{-1/2}$ , but the correlations remain the same. Without mosaicing (WCDH) the resolution in  $\ell$  is restricted to  $\sim 2\pi D$ , thus the individual determinations are required to be highly correlated. The error on the highest  $\ell$  bins is still dominated by the small number of

independent samples, in this case 16. Increasing the oversampling in the angular direction (and the observing time) can reduce this error to about 23%, hardly worth the extra time compared to including a different pointing.

The  $\mathcal{S}_A$  are estimates of the power spectrum *convolved with the window function*  $W_A(u)$ . Given a theory it is straightforward to compare to the data once the window functions are known, and we discuss this in §7. However one could ask whether (or how much) cosmological information has been lost due to the convolution or if the information is still present in the correlated visibilities. One way of answering this question is to attempt to perform an approximate (theory independent) deconvolution.

The simplest (“direct”) method is to assume that  $S(u) = \text{constant}$  through the window, so that  $S(u) \approx \mathcal{S}_A / \int u du W_A(u)$  with  $W_A(u) = \sum_i E_{Ai} W_{ii}(u)$ . (Alternatively one could assume that  $u^2 S(u) = \text{constant}$ , which leads to a similar expression.) For the window function of Eq. (4) we have  $\int d^2u \tilde{A}^2(u) \simeq 0.585 D^{-2}$ . As we show in Fig. 5, this technique works surprisingly well for DASI, even though the FWHM of each window is  $\Delta\ell \sim 100$ , over which scales we can expect power spectra to change significantly. For a CDM power spectrum for example, the approximation above induces a systematic 10% error (at worst) due to the window function “washing out” the peak structure.

To avoid this problem, we can attempt to perform the deconvolution by an iterative procedure. Recall that we are trying to constrain the power spectrum, while our measurements are the spectrum convolved with a positive semi-definite kernel – the window function. In this situation Lucy’s method (Lucy 1974) can be used. We have implemented Lucy’s algorithm, following Baugh & Efstathiou (1993), including a coupling between different bins and a regularization of the iteration. As they found, the final result is not sensitive to the mechanism chosen.

To briefly re-cap the method: we think about the deconvolution problem, following Lucy (1974), first in terms of probability distributions. If we denote by  $p(x)$  the probability of measuring a quantity  $x$  and  $p(y|x)$  the conditional probability of measuring  $y$  given that  $x$  is true then

$$p(y) = \int p(y|x)p(x)dx \quad (19)$$

which is a convolution integral. We wish to estimate  $p(x)$  given observations  $p^{\text{obs}}(y)$ . We start the  $r$ th iteration with an estimate  $p^r(x)$  of  $p(x)$  and predict  $p^r(y)$  using Eq. (19) assuming  $p(y|x)$  is known. Writing the inverse of Eq. (19), for  $p(x)$ , using the observed  $p^{\text{obs}}(y)$  and rewriting  $p(x|y)p(y) = p(y|x)p(x)$  leads us to the iterative expression for  $p^{r+1}(x)$ :

$$p^{r+1}(x) = p^r(x) \frac{\int (p^{\text{obs}}(y)/p^r(y)) p(y|x)dy}{\int p(y|x)dy} \quad (20)$$

where the denominator is unity. The iterative method we use takes this expression over with the replacements  $p(y) \rightarrow \mathcal{S}_A$ ,  $p(x) \rightarrow f(u) \equiv u^2 S(u)$  and  $p(y|x) \rightarrow u^{-1} W_A(u)$ . Approximating the integrals as sums equally spaced in  $u$  we have the iterated pair of equations:

$$\mathcal{S}_A^r = \sum_a f^r(u_a) u_a^{-1} W_A(u_a) \Delta u \quad (21)$$

$$f^{r+1}(u_a) \equiv f^r(u_a) \frac{\sum_i (\mathcal{S}_A^{\text{obs}}/\mathcal{S}_A^r) u_a^{-1} W_A(u_a)}{\sum_i u_a^{-1} W_A(u_a)} \quad (22)$$

To make the iteration converge more stably we in fact replace only a fraction  $\epsilon$  of  $f^r$  with  $f^{r+1}$  on each step, and average the  $f^r(u_a)$  using a 2nd order Savitsky-Golay filter of length (2, 2). The final result is insensitive to the details of this procedure, the number of bins chosen for  $u_a$  etc.



We show in Fig. 5 results of a deconvolution assuming that 16 independent patches of sky were observed, each for 1 day. We can see that the deconvolution works well, with good resolution in  $\ell$  and no bias over the scales where DASI has sensitivity. Thus we expect that no important cosmological information has been lost by the convolution procedure. The points are highly correlated, but we do not show the correlations on the Figure (all correlations were included in the analysis). The error bars are so large because they are the computed from the variance *allowing all other bins to vary freely*.

Though the example here was for a single frequency channel, the generalization to multiple frequencies is straightforward and can in principle allow even finer sub-band resolution.

Finally we remark that obviously a statistical comparison of a given model to the data should be done with the  $\mathcal{S}_A$ . The correlations of the  $\mathcal{S}_A$  can be computed for any given theory (e.g. Table 2). This allows a full likelihood analysis to be done, and is the route which should be taken when comparing DASI data to a specific theory. This is what we shall discuss now.

## 7. Radical Compression

To constrain theories using interferometer data is much easier than in the case of single dish data, thus many of the powerful techniques developed for the latter case are not needed. The primary reason for this is that interferometers work directly in the  $\ell$ -space of theories. It is straightforward to perform “radical compression” (Bond, Jaffe & Knox 1998) of an interferometer data set and quote a set of bandpowers along with their full noise covariance matrix and window functions. We shall develop this idea briefly in this section.

We now reintroduce the multi-frequency nature of the data set that has been suppressed during most of this paper. For DASI we can work with 10×1GHz channels which we shall label with a greek subscript. Following Dodelson (1997; see also White 1998) we imagine that our visibility signal  $V_\alpha$  at each point in the  $u$ - $v$  plane is a sum of contributions with different frequency dependences:  $V_a = \sum_A \theta^A V_a^A$ . Let  $A = 0$  be the CMB contribution, whose frequency dependence will be  $V^0 = (1, 1, \dots)$  for observations at DASI frequencies. At each frequency,  $a$ , and visibility position,  $i$ , the signal is the convolution of the sky with an aperture  $\tilde{A}_i^a$  which will be of the form of Eq. (4) with the central  $u$  and  $D$  varying by the inverse of the observing wavelength. If each visibility has noise  $N_{ab}^{(i)}$  we can estimate the CMB component  $\theta^0$  by minimizing

$$\chi^2 = \sum_{ab} \sum_{AB} (V_a^{\text{obs}} - \theta^A V_a^A) N_{ab}^{-1} (V_b^{\text{obs}} - \theta^B V_b^B) \quad (23)$$

where we have suppressed the visibility index  $i$ . Solving  $d\chi^2/d\theta^A = 0$  amounts to taking a linear combination of the frequency channels  $\theta_i^0 = \sum_a c_a V_a^{\text{obs}}$  with

$$c_a = \sum_A \left( \sum_{bc} V_b^0 N_{bc}^{-1} V_c^A \right)^{-1} \sum_d V_d^A N_{ad}^{-1} \quad (24)$$

While formidable this expression reduces to the well known least-squares weighting in the limit  $N_{ab} = \sigma_a^2 \delta_{ab}$ :

$$c_a = \sum_{Ab} \left( \frac{V_b^0 V_b^A}{\sigma_b^2} \right)^{-1} \frac{V_a^A}{\sigma_a^2} \quad (25)$$

Now we simply replace  $V_i$  with  $\theta_i^0$  and  $\tilde{A}_i$  with  $\sum_a c_a \tilde{A}_{ia}$  to generalize Eq. (17). The generalized  $\mathcal{S}_A$  can be easily calculated from the data, and the expectation values and distribution can be calculated for any

theory once the window function and noise properties are given. Supplying this set would be an ideal way to release the DASI data for the purposes of model fitting.

## 8. Conclusions

We have shown how one can implement the formalism of WCDH in the case of a single stare of the DASI instrument. We have discussed making maps, filtering the data and reconstructing the anisotropy power spectrum. Our results suggest that with  $\sim 1$  month of data, DASI could provide significant constraints on theories of structure formation.

We would like to acknowledge useful conversations with Alex Szalay and thank Tim Pearson for comments on a draft of this work.

## REFERENCES

- Baugh C.M., Efstathiou G., 1993, MNRAS, 265, 145
- Bennett C.L., et al., 1996, ApJ, 464, L1
- Bennett C.L., Turner M., White M., 1997, Physics Today, November, 32
- Bond, J.R., Jaffe, A.H., Knox, L., 1998, Phys. Rev. D57, 2117
- Bunn, E.F., Hoffman, Y., Silk, J., 1996, ApJ, 464, 1
- Dewdney, A.K., 1985, “Computer Recreations”, Scientific American, Dec 1985, pp. 16–26
- Dodelson S., 1997, ApJ, 482, 577
- Halverson N., Carlstrom J.E., Dragovan M., Holzzapfel W.L., Kovac J., 1998, *In'l Symp. on Astronomical Telescopes and Instruments*, SPIE 3357
- Lucy, L.B., 1974, AJ, 79, 745
- Popieszalski, M.W., Proc. of 23rd European Microwave Conference, Madrid, Spain September 1993, p. 73
- Tegmark, M., 1996, MNRAS, 280, 299
- Tegmark, M., 1997, Phys. Rev. D55, 5895
- Tegmark, M., et al., 1998, ApJ, 499, 555
- White, M., 1998, Phys. Rev. D57, 5273
- White, M., Carlstrom, J., Dragovan, M., Holzzapfel, S.W.L., 1999, ApJ, 514, 12

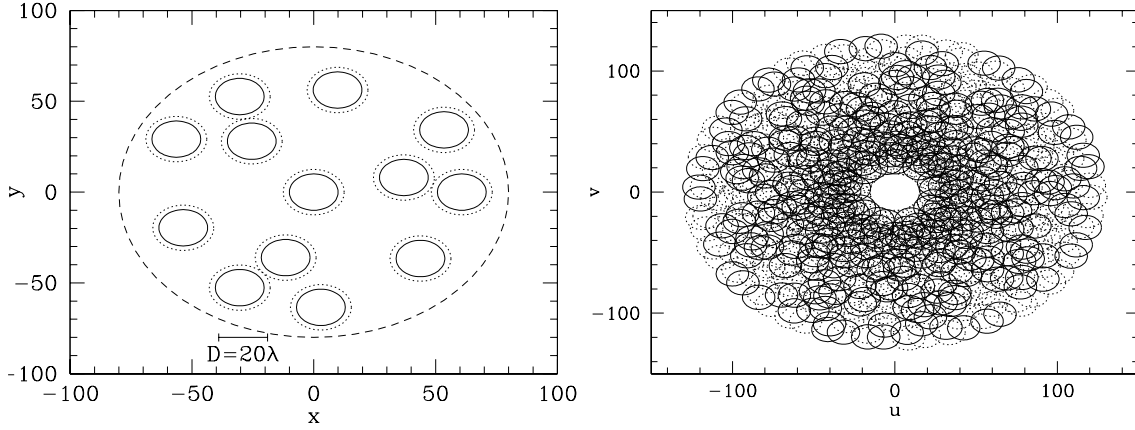


Fig. 1.— (a) The positions of the dishes for DASI. Each dish has an effective optical diameter  $D = 20\lambda$  with  $\lambda = 1\text{cm}$  (solid lines). The physical size of the dishes is 25cm (dotted lines) and the base plate for DASI is 1.6m in diameter (dashed line). (b) The positions at which visibilities will be measured in 1 “stare” of DASI. The circles show apertures of radius 10 (roughly the half power point of the beam profile). Each visibility consists of an independent real and imaginary part. Solid lines indicate where data will be taken, the dotted lines indicate points constrained by symmetry of the transform.

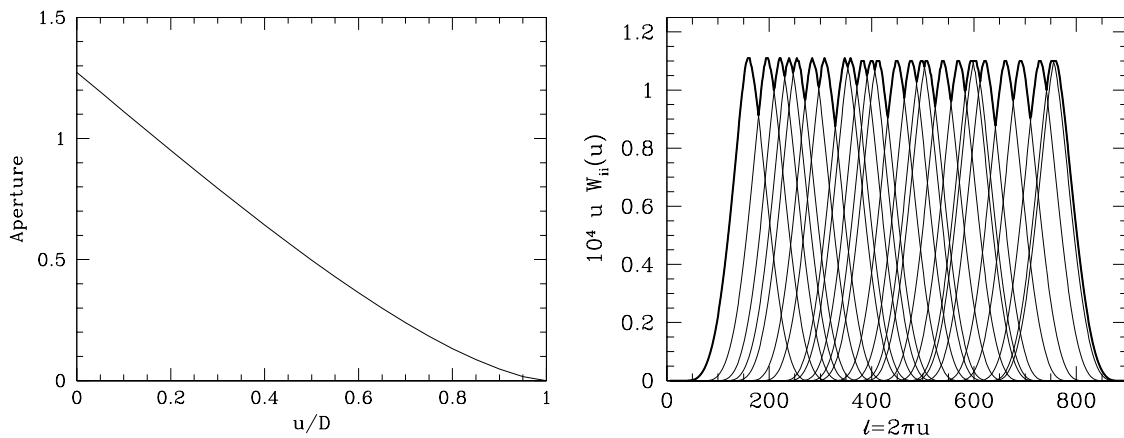


Fig. 2.— (a) The aperture function  $\tilde{A}$  described in the text (Eq. 4). For DASI,  $D = 20$ . (b) The window functions for the 26 baselines of DASI.

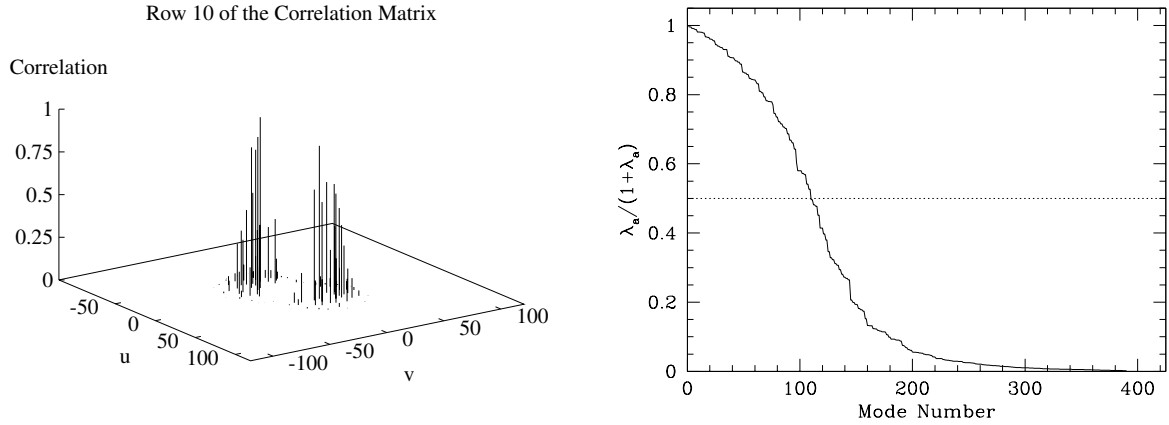


Fig. 3.— (a) One row of the signal correlation matrix, plotted in the  $u - v$  plane. (b) the signal-to-noise eigenvalues  $\lambda_a$  for the *real* part of the visibilities. For every real  $\lambda_a$  there is an independent imaginary mode with the same signal-to-noise. All calculations assume a scale-invariant COBE normalized spectrum.

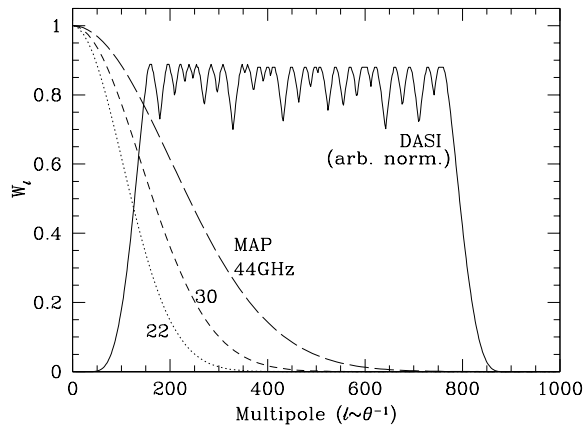


Fig. 4.— The window functions for *MAP* and *DASI*, showing the complementarity in angular scale of the two instruments at low frequency. The *MAP* data will provide large-scale information over the whole sky which can be used when making maps with *DASI*, which is sensitive to the small angular scales which *MAP* cannot resolve.

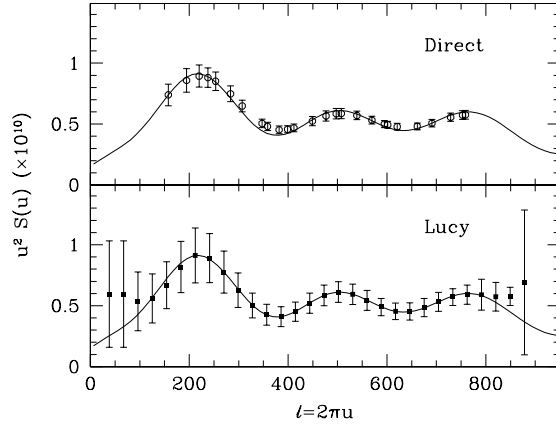


Fig. 5.— Estimates of the power spectrum obtained from simulated data from 16 independent DASI fields, each observed for 1 day. (Upper) The open circles indicate estimates obtained by assuming  $S(u) = \text{constant}$  through the window function. (Lower) The solid squares are from Lucy’s method. The points are highly correlated (see text).

$x$ (cm)	$y$ (cm)
+00.00	+00.00
+60.76	+00.00
+53.47	+34.25
+36.98	+08.04
+09.77	+56.21
−30.38	+52.62
−56.40	+29.18
−25.45	+28.01
−53.56	−19.64
−30.38	−52.62
+02.93	−63.43
−11.53	−36.05
+43.79	−36.57

Table 1: The positions of the centers of the horns on the DASI base plate for the optimal configuration described in §3.

$\ell_i = 2\pi u_i$	158	220	253	307	358	399	449	497	539	595	621	691	753
158	100	36	9	0	0	0	0	0	0	0	0	0	0
220	36	100	72	14	1	0	0	0	0	0	0	0	0
253	9	72	100	45	6	0	0	0	0	0	0	0	0
307	0	14	45	100	45	11	0	0	0	0	0	0	0
358	0	1	6	45	100	52	10	1	0	0	0	0	0
399	0	0	0	11	52	100	39	6	0	0	0	0	0
449	0	0	0	0	10	39	100	35	8	0	0	0	0
497	0	0	0	0	1	6	35	100	34	5	1	0	0
539	0	0	0	0	0	0	8	34	100	20	9	0	0
595	0	0	0	0	0	0	0	5	20	100	33	4	0
621	0	0	0	0	0	0	0	1	9	33	100	12	1
691	0	0	0	0	0	0	0	0	0	4	12	100	14
753	0	0	0	0	0	0	0	0	0	0	1	14	100
$\sigma$	0.49	0.40	0.37	0.33	0.31	0.29	0.28	0.27	0.26	0.26	0.26	0.26	0.26

Table 2: The  $\mathcal{S}_A$  correlation matrix,  $C_{AB}/\sigma_A\sigma_B$  with  $\sigma_A \equiv C_{AA}^{1/2}$ , for every *second* estimate of the power spectrum from a *single pointing* of DASL. Correlations are listed as percentages. The final row shows the relative error on the power spectrum in the bin. Since the error is dominated by sample variance, for  $N$  such pointings  $\sigma$  is reduced by  $N^{1/2}$ . All calculations assume a scale-invariant COBE normalized spectrum.